Korean J. Chem. Eng., 33(6), 1922-1930 (2016)
DOI: 10.1007/s11814-016-0040-7

pISSN: 0256-1115
eISSN: 1975-7220

Crystallization kinetics for carbon dioxide gas hydrate in fixed bed and stirred tank reactor

Asheesh Kumar*, Dishant Khatri, Ju Dong Lee***, and Rajnish Kumar*,†**

*Chemical Engineering and Process Development Division, National Chemical Laboratory, Pune, India
**Department of Chemical Engineering, Indian Institute of Technology-BHU, Varanasi 221005, India
***Offshore Plant Resources R&D Center, Korea Institute of Industrial Technology,
1274 Jisa-dong, Gangseo-gu, Busan 618-230, Korea
(*Received 4 December 2015 • accepted 4 February 2016*)

Abstract−The phase change from germ nuclei to growth nuclei and subsequent volume transformation in a crystallization process was modeled by Avrami equations. The phase change during the hydrate formation was fitted with the classical Avrami model by utilizing gas uptake data. The idea is to understand the difference in growth behavior of hydrate crystals when in small pores compared to a stirred tank reactor which does not pose any physical restrictions to hydrate growth. The parameters n and k of the Avrami equation were determined explicitly for CO_2 hydrate formation.

Keywords: Gas Hydrates, Avrami Equation, Kinetics, Fixed Bed, CO_2 Capture & Sequestration

INTRODUCTION

Gas hydrates, or clathrate hydrates, are the ice-like nonstoichiometric crystalline compounds that are formed when small gases or liquid molecules (guest) are entrapped within cages formed by hydrogen bonded water (host) molecules at high pressure and low temperature [1,2]. Apart from its importance as an energy resource (natural gas hydrate is a potential source of methane gas, exists across the globe in marine environment and in permafrost region), gas hydrates have been identified as a suitable material for H_2 storage and CO_2 capture and sequestration [3-5]. CO_2 capture and separation from a flue gas ($CO_2 : N_2$ mixture) and fuel gas ($CO_2 : H_2$ mixture) by clathrate hydrates formation, also known as HBGS (Hydrate based gas separation) process has been found to be attractive due to its environmental friendly approach [6-11]. HBGS process is essentially a multistage hydrate formation and decomposition cycle very similar to pressure swing/temperature swing adsorption [12]. In this process a gas mixture having carbon dioxide is brought in contact with water so that CO_2 preferentially forms hydrates, resulting in CO_2 separation from its mixture [13-15]. The separation efficiency is a function of lower induction time, faster growth kinetics and higher water to hydrate conversion [2]. However, for this process to be commercially feasible, the above three factors need to be optimized at a temperature and pressure not far from ambient (restricted by thermodynamics). The enclathration starts at the gas-water interface and water to gas contact plays an important role in gas hydrate formation kinetics. It has been observed that using porous media for water to gas contact is more economical than having a stirred tank configuration; it enhances the hydrate growth kinetics and water to hydrate conversion while reducing the induction time [2,16-19]. In hydrate crystallization, induction time is an important characteristic of the kinetics which is experimentally accessible [20]; however, it is extremely difficult to measure the rate of nucleation through experiments, moreso because nucleation is a stochastic phenomenon and upon initial hydrate nucleation, growth and nucleation happen simultaneously [10]. Hydrate formation is an exothermic process in which crystallization is characterized by nucleation followed by growth and agglomeration [3,21]. To maintain the hydrate growth, gas molecules and/or water molecules have to diffuse through the growing hydrate layer.

In case of a stirred tank reactor, the enclathration starts at the gas-water interface and progresses towards bulk water phase, as gas hydrate formation depends on water to gas contact area [22]. For a fixed bed reactor, porous media maximizes the gas to water interface, which is quite conducive for the hydrates to nucleate and grow within the pores of the media (intra pore hydrates) as well as between the particles (inter pore hydrates). However, effective diffusion of hydrate forming gases and partial plugging of pores due to quick hydrate formation needs to be understood. At the same time, smaller pore sizes are known to change the thermodynamic boundary and push the three phase equilibria to extreme conditions, thus reducing the effective driving force for better growth kinetics.

In addition, CO_2 sequestration in the geological storages as hydrate has also been considered a potential application where thermodynamic conditions suitable for CO_2 hydrate formation exist. Recently, Sun and Englezos simulated the lab scale injection of CO_2 in porous media for sequestration or storage purpose [23]. In geological storages through hydrate formation, it is essential to understand hydrate formation kinetics/hydrate growth mechanism which is not possible to observe visually.

In the current work, the Avrami model is employed to get the

†To whom correspondence should be addressed.
E-mail: k.rajnish@ncl.res.in

idea of hydrate growth mechanism in porous medium. Avrami [24-26] developed a theory of kinetics of phase change with the experimentally supported assumptions that the new phase is generated by germ nuclei which already exist in the old phase, which is more or less similar to the memory effect in gas hydrates. The quantitative relations between the density of germ nuclei, growth nuclei and transformed volume are derived in terms of a characteristic time scale for any given substance or process [24]. As hydrate formation is a crystallization process, this equation in the same or modified form can be used to explain the kinetics of gas hydrate formation. Kashchiev and Firoozabadi developed a model for hydrate nucleation and growth kinetics based on classical nucleation and crystallization principles for single component gas hydrate systems [20,27]. To explain the nucleation and growth of gas hydrates on ice surface, Moudrakovski et al. used the Avrami-Erofeyev equation which emphasizes the importance of nucleation step for Xe hydrate formation [28]. Falenty and Kuhs showed that the gas hydrate decomposition reaction outside the regime of self-preservation can be described by an Avrami-type process [29]. Susilo et al. also showed that methane uptake curves fit well with Avrami equation. The Avrami equation correlates the experimental data of initial reaction stage (where nucleation and intrinsic kinetics control the reaction) and fits quite well for the hydrate conversion during this stage. The Avrami exponent (n, discussed later) was found to be 0.5, which suggests that hydrate nucleated instantaneously and grew in one dimension with methane diffusing into ice and hydrate phase [30]. Nambiar et al. also carried out kinetic modeling of hydrate formation in porous media using the Avrami model and found that this model fits the hydrate growth kinetics very well up to 40 minutes of hydrate growth for different porous media like silica sand, polyurethane foam, and cellulose foam for pure CO_2, CO_2/H_2 and $CO_2/H_2/C_3H_8$ gas mixtures. The Avrami exponent (n) in silica sand media was found to be 0.68, 0.38 and 0.69 for CO_2, CO_2/H_2 and $CO_2/H_2/C_3H_8$ gas mixtures, respectively. However, it was 0.89 and 0.86 for polyurethane foam and cellulose foam, respectively, using $CO_2/H_2/C_3H_8$ gas mixture [31].

In the present work, the gas uptake data for hydrate formation was obtained at isothermal conditions and hydrate growth phase after induction time were fitted with the modified Avrami equation. For such a system, the crystallization kinetics model for gas hydrate formation can be explained by using well known Avrami equation [24-26] for the initial growth kinetics. The Avrami model shown below has three important parameters:

$$\alpha = 1 - \exp(-k_1 t^n) \text{ or } \ln[-\ln(1-\alpha)] = n \ln t + \ln k_1 \quad (1)$$

Here α represents water to hydrate conversion ratio at time t, k is the overall crystallization rate constant (i.e., it contains contributions from both nucleation and growth) with the subscript indicating the growth stage, n is the Avrami exponent which represents the hydrate nucleation and growth during gas hydrate formation [32,33]. The n-value increases with dimensionality of the growth, starting from unity for a free linear growth up to 3 for a three-dimensional growth. Instantaneous nucleation does not contribute any additional value to n; however, sporadic nucleation does. The maximum n-value is 4 when the crystal growth is in three-dimensions and sporadic nucleation is expected [34]. Mass transfer resistance such as diffusion-controlled growth reduces the value of n, typically by half [32]. In a packed (fixed) bed reactor, the resistances due to pore diffusion might be higher, while resistance to film diffusion is expected to be lower; it is thus expected that Avrami coefficients n and k would give better insight for hydrate growth in packed bed medium. The gas hydrate formation or nucleation occurs in the metastable region, when temperature reaches below the equilibrium temperature. The general S-shape curve is a characteristic of the water to hydrate conversion with time, which is the same as proposed by Avrami (1937) to explain the kinetics of phase change where they have shown the same transformation-time curve at lower supercooling temperature. Avrami model assumes constant density of the hydrate phase, thus making it independent of the amount of hydrate formed. The model assumes that the nucleation of a product phase is random and no preferential nucleation on walls or packing material is possible, and the rate of the phase change (growth of the crystal) is constant. The rate of growth can be calculated, provided that the nucleation probability is known as a function of time [24-26]. The fact that for the first few minutes of hydrate formation intrinsic kinetics is dominant makes the Avrami equation of crystallization a suitable model for gas hydrate formation. Also, compared to hydrate formation in a stirred tank reactor, fixed bed medium ensures that there is no bulk hydrate formation, and thus has limited mass transfer resistance even after initial hydrate growth. In the current study, the Avrami model is used to determine the rate constant of CO_2 hydrate formation and its mechanism in fixed bed reactor compared with a stirred tank reactor. The influence of surfactant (SDS) on gas hydrate formation is also explained by the value of adjustable coefficients in Avrami equation.

EXPERIMENTAL SECTION

The experimental data of the fixed bed apparatus were taken from our earlier paper [35], and for gas uptake data from stirred tank reactor, fresh experiments were carried out. Detailed procedure for experiments carried out in the fixed bed setup is given in Kumar et al [35]. A schematic of the stirred tank setup is shown in Fig. 1. It consists of a 400 cm^3 SS-316 high-pressure hydrate crystallizer (CR) (Berghof-192-BJ-2012, Germany). The top cover plate of the crystallizer has six ports each equipped with a Swagelok connector. These ports are used for inserting a thermocouple, supplying gas (inlet), vent and safety valve, gas sample extraction, liquid sample extraction and pressure transducer. The resistance temperature detectors (Pt-100) with ±0.1 K accuracy are used to measure the temperature of the reactor contents. All pressure measurements are made with pressure transducers (make: Wika-S10), with a range of 0-250 bar and accuracy of 0.075% of the span. The crystallizer is immersed in a temperature controlled water bath containing a 40/60 wt% ethylene glycol/water mixture, which maintains the temperature in the hydrate crystallizer constant. The setup is equipped with a gas chromatograph (GC-2014AT, Shimadzu) to measure the composition of the gas phase in the crystallizer. In this stirred tank reactor, experiments were carried out with a fixed amount of water (120 mL) at constant temperature of ~274.5 K & 3.5 MPa pressure and at three different stirring rates of 200, 400 and 600 rpm [36].

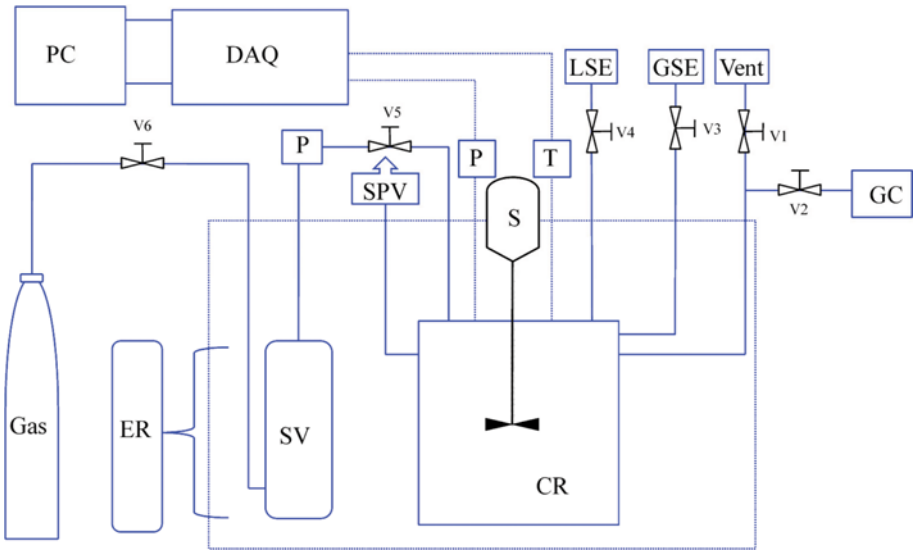

Fig. 1. Schematic of experimental setup: Stirred tank reactor.

CR. Crystallizer
SV. Supply vessel
GC. Gas chromatography
P. Pressure transducer
T. Thermocouples
S. Stirrer
DAQ. Data acquisition system
ER. External refrigerator
SPV. Safety pressure valve
GSE. Gas sample extraction
LSE. Liquid sample extraction

As given in the literature, the Avrami model has been used for fixed bed reactors where adsorption takes place [37,38].

It is expected that the Avrami model would provide a good fit of the experimental data during the initial stage of hydrate growth, beyond which mass transfer effect dominates the crystallization rate. The calculation of n and k is performed by fitting the data in a double-logarithmic plot (Sharp-Hancock plot) for first stage of hydrate formation. The Sharp-Hancock plot should give a straight line where the slope refers to n and the intercept corresponds to ln k. Therefore, the correlation coefficient (R^2) of the fit has to be very high if a good fit is obtained. The Avrami equation in its simplest form gives a value of α equal to 0 when the crystallization time is 0 (i.e., before the induction time) and values more than zero at any time (t) implies that hydrate growth has started. Therefore, in mathematical terms the equation is only defined when crystallization starts. The Avrami equation cannot account for a time period where there is no crystallization. Hence, induction time, t_0, must be subtracted from the absolute time (t) or, in other words, time count must start from time equal to t_0. Therefore, a minor modification has to be introduced into the classical Avrami equation in order to take into consideration the experimental induction time t_0. Hence the modified Avrami equation becomes

$$\ln[-\ln(1-\alpha)]=\ln k+n\ln(t-t_0) \text{ or } \alpha=1-\exp[-k\times(t-t_0)^n] \quad (2)$$

where α is water to hydrate conversion at time $t-t_0$. The regressed values of n and k are given in Table 1.

Mean absolute percentage error (MAPE) is used to predict the error in the Avrami model that fits the hydrate conversion ratio data during the first stage or initial hydrate formation stage.

The following formula is used for calculating the MAPE (%):

$$\text{MAPE}=\frac{\sum_{t=1}^{n}\frac{E_t-F_t}{E_t}}{n}\times 100 \quad (3)$$

Table 1. Avrami parameters obtained from sharp Hancock plot

System	n	Standard error	k	Standard error	Adj. R-square value
(A) Silica gel (60-120)/water/CO_2 system	0.934	0.0067	0.000881	0.000026	0.9950
(B) Silica gel (100-200)/water/CO_2 system	0.930	0.0051	0.001675	0.000099	0.9947
(C) Silica gel (230-400)/water/CO_2 system	0.924	0.0043	0.004873	0.00026	0.9962
(C)/SDS (500 ppm)/CO_2 system	0.984	0.0170	0.003400	0.000210	0.9917
(C)/SDS (2000 ppm)/CO_2 system	0.920	0.0064	0.004900	0.000120	0.9982
(C)/SDS (4000 ppm)/CO_2 system	0.925	0.0215	0.010000	0.000490	0.9959
Water/CO_2 system (stirred tank reactor) 200 rpm	1.100	0.0110	0.001590	0.000031	0.9966
Water/CO_2 system (stirred tank reactor) 400 rpm	0.970	0.0085	0.005240	0.000119	0.9947
Water/CO_2 system (stirred tank reactor) 600 rpm	0.980	0.0014	0.006270	0.000140	0.9954
Water/SDS (500 ppm)/CO_2 system (stirred tank reactor) 400 rpm	0.845	0.0084	0.007140	0.000176	0.9901

Table 2. The error in the Avrami model is expressed in mean absolute percentage error (MAPE) for all the systems used in this study

S. No.	System	Time for Avrami model prediction (min)	MAPE (%)
1	(A) Silica gel (60-120)/water/CO_2 system	150	10.4
2	(B) Silica gel (100-200)/water/CO_2 system	30	5.0
3	(C) Silica gel (230-400)/water/CO_2 system	50	9.0
4	(C)/SDS (500 ppm)/CO_2 system	75	9.6
5	(C)/SDS (2000 ppm)/CO_2 system	75	8.2
6	(C)/SDS (4000 ppm)/CO_2 system	30	7.8
7	Water/CO_2 system (STR) 200 rpm	30	2.3
8	Water/CO_2 system (STR) 400 rpm	18	1.6
9	Water/CO_2 system (STR) 600 rpm	12	3.0
10	Water/SDS (500 ppm)/CO_2 system (STR) 400 rpm	30	2.0

where E_t and F_t represent the experimental and Avrami fit data, respectively, for hydrate conversion ratio. The calculated MAPD is presented in Table 2.

RESULTS AND DISCUSSION

To evaluate the kinetics of gas hydrate formation, the gas uptake curves were fitted to the crystallization model (Avrami equation) for initial stage of hydrate formation. The regressed values of n and k are given in Table 1 which was obtained from Sharp-Hancock plot. It contains data for three different silica gel media (different mesh size), silica gel with three different concentrations of SDS (anionic surfactant) and for stirred tank reactor with and without SDS.

The value of n is given in Table 1 (calculated using Eq. (2)) and as a first approximation considered to be composed of two terms: $n=n_d+n_n$ where n_d represents the dimensionality of the growing crystals and n_n represents the time dependence of the nucleation. The n_d can have only the integer numbers 1, 2 or 3 corresponding to one-, two- or three-dimensional entities that are formed [39]. In the case of polymers, the value of n_d is either 2 or 3, as they represent axialites (two-dimensional lamellar aggregates) and spherulites (superstructural three-dimensional aggregates of radial lamellae), respectively, while in the case of gas hydrate it is expected to vary between half and one depending on the degree of mass transfer resistance for gas diffusion [30]. The value of n_n should be either 0 or 1, where 0 corresponds to instantaneous nucleation and 1 to sporadic nucleation. However, since in many cases the nucleation may be in between completely instantaneous or completely sporadic. This can lead to a non-integer value of n [40-42]. In those cases n_n can have a value of 0.5, which indicates Fickian dependence (following Fick's law) of growth with the square root of time [42]. The typical Avrami plots for packed bed reactor are shown in Figs. 2 and 3. The correlations from Avrami model to the measured conversion rate are shown in Fig. 4 (for three silica gel media) and Fig. 5 (for silica gel media with various concentration of SDS). In a packed bed reactor (using porous silica gel), hydrate formation depends on the wettability of the medium, water and gas saturation in the pores, the size of the pores, total surface area of medium and so forth [17,35]. The mass transfer resistance offered is due to pore diffusion and film diffusion.

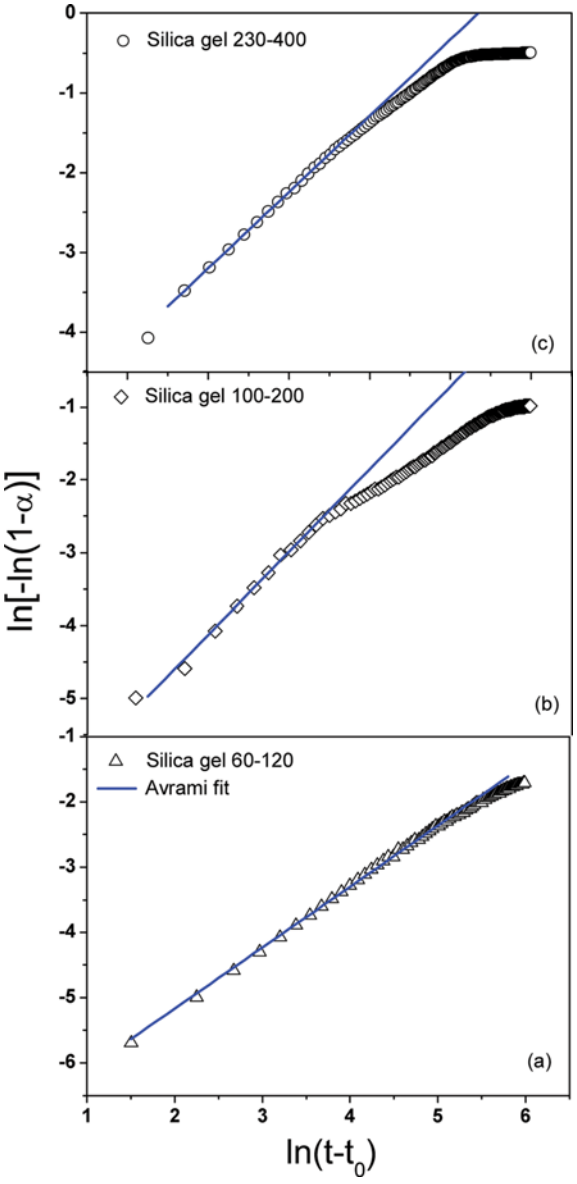

Fig. 2. Avrami plot for fixed bed reactor where three types of silica gels was used. Dotted line corresponds to the data calculated using Avrami equation and solid line corresponds to the linear fit. The regressed parameters (n and k) are given in Table 1.

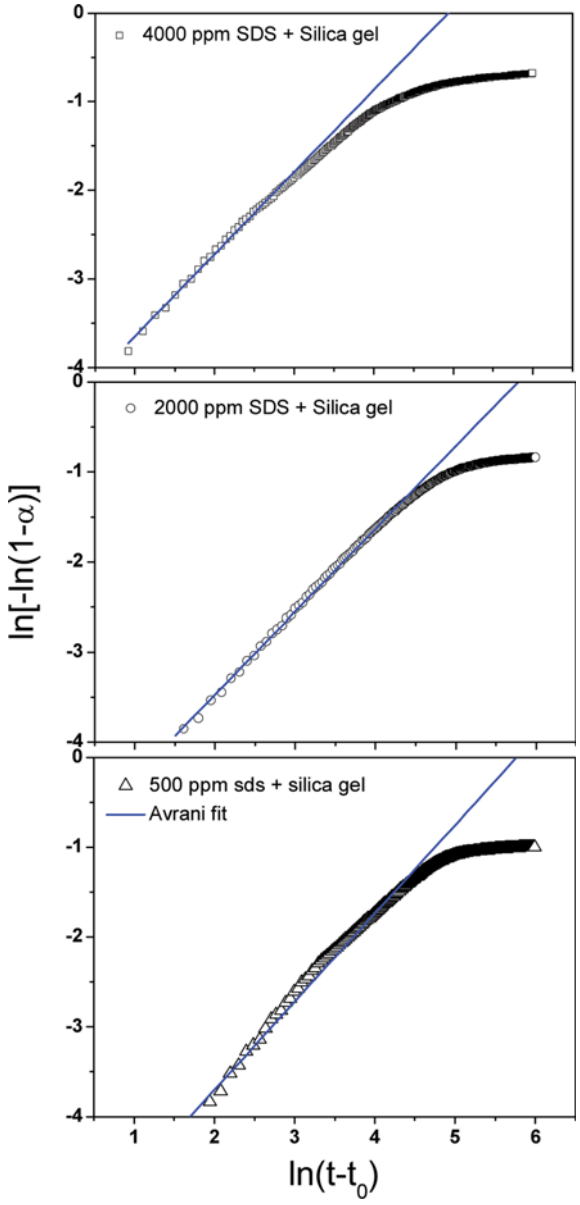

Fig. 3. Avrami plot for fixed bed reactor, in which 230-400 mesh type of silica gel with different concentration of SDS was used. Dotted line corresponds to the data calculated using Avrami equation (Eq. (2)) and solid line corresponds to the linear fit. The regressed parameters (n and k) are given in Table 1.

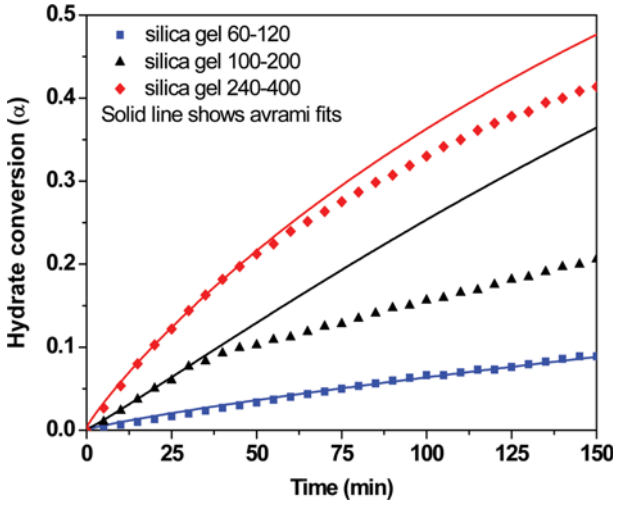

Fig. 4. Hydrate conversion for three different silica gels correlated well with Avrami model.

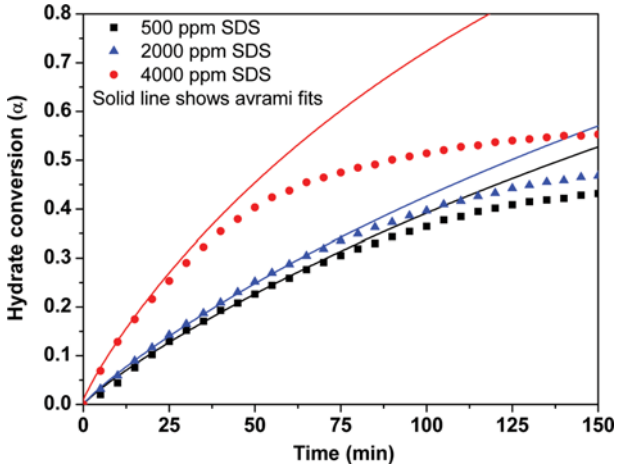

Fig. 5. Hydrate conversion for 230-400 mesh type of silica gel with different concentration of SDS (500, 2,000 and 4,000 ppm) correlated well with Avrami model for first stage.

In the present work, pore size of all the three types of silica gel used in this study was quite similar; however, it differs in particle size and exposed specific surface area [35]. As seen in Fig. 2, the linear correlation fits for a longer time (~150 min) in type A silica gel (60-120 mesh), which has largest particle size distribution and smaller specific surface area (compared to type B (100-200 mesh) and C (230-400 mesh) silica gel), while in other two silica gels the linearity vanishes after some time (~30 min), where the model slightly overestimates the data (also refer Table 2). This may be ascribed to the role of resistance of hydrate film formed around inter and intra pores.

As seen in Figs. 4 and 5, the Avrami model fits the hydrate conversion ratio data during the first stage quite well (initial hydrate formation; refer to Table 2) [30]. At the end of the first stage, effects of mass transfer resistance come into picture and rate of hydrate formation decreases. As the layer of nuclei is formed at the interface (solid-liquid-gas) and the interfacial area between reactant and products decreases or pores are blocked, there is much less water to gas contact, which results in slower kinetics. Fig. 4 represents the hydrate conversion ratio for three different silica gels, which shows good correlation with Avrami model. As seen in Fig. 4, the slopes of all Avrami plots of the system are almost parallel to each other with an n value at around ~0.93. For a system where there is no resistance (free growth) with linear growth in one dimension and instance nucleation, the expected value of n is one [30]. The observed n value of 0.93 shows that for the first 30 minutes hydrate grows linearly in one dimension and mass transfer resistance is quite less, which shows that a for a fixed bed arrangement there is unhindered hydrate growth for the first 30 minutes of hydrate formation (sI hydrate) [43]. Susilo et al., also applied the Avrami model

for sI hydrate where methane hydrate was formed in fine crushed ice. In ice-methane system, no gas diffusion through a liquid film exists; in absence of any mass transfer resistance n-value should be closer to one. However, in that study it was found that the n value is closer to 0.5, which is expected as ice to hydrate transformation cannot be called a classical crystallization process [30]. The value of K (rate constant) is in the good agreement with the experimental results shown in literature [35]. As seen in Table 1, the value of k is of order 10^{-3}, which increases with increase of surface area of silica gel (shown in previous paper [35]). The k value of CO_2 hydrate formation in silica gel of mesh size 100-200 was found almost twice compared to 60-120 mesh silica gels. However as seen in Table 1, the n value of system does not change drastically with small change in pore volume studied for this work.

Similar types of results were obtained when various concentration of SDS were added with C type of silica gel (Figs. 3 and 5). As seen in Table 1, at 500 ppm SDS concentration there is a slight increment in the value of n compared to hydrate formation without SDS. However, as we increased the concentration of SDS from 500 to 4,000 ppm, n value remained more or less constant. This result is expected due to fast initial hydrate growth rate at higher SDS concentration followed by suggestion that at higher SDS concentration of the 2,000 and 4,000 ppm SDS concentration enhances the initial rate of gas hydrate formation significantly compared to 500 ppm surfactant (see Table 1), which creates less concentration gradient around the pore as well as in the pore. Hence, it reduces the further diffusion of gas and thus reduces the n value slightly.

Hydrate crystal growth may actually consist of three stages (represented in Fig. 6). The first stage occurs rapidly and dominates the crystallization growth. It is primary crystallization process where the radial growth from the center of nuclei is observed, most probably forming a needle-like crystal (1D), as suggested by n value closer to one. The secondary growth stage is slower and the crystallization process is now affected by the mass transfer resistance posed by the hydrate crystals, which forms in interparticle spaces of

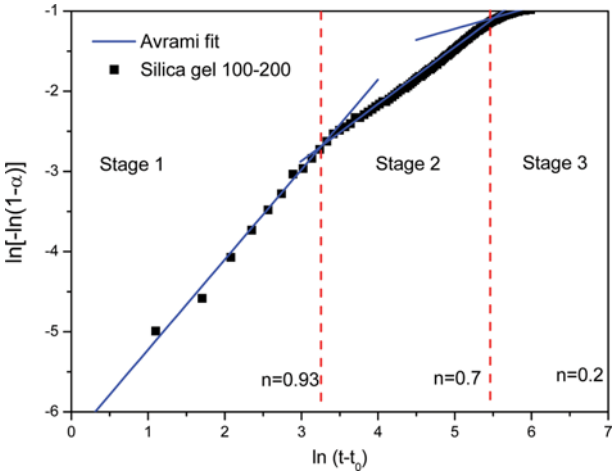

Fig. 6. Three stage Avrami plot for fixed bed reactor with 100-200 mesh silica gels. Dotted line corresponds to the data calculated using Avrami equation, and solid line corresponds to the linear fit. Stages correspond to time interval where a type of resistance is dominant.

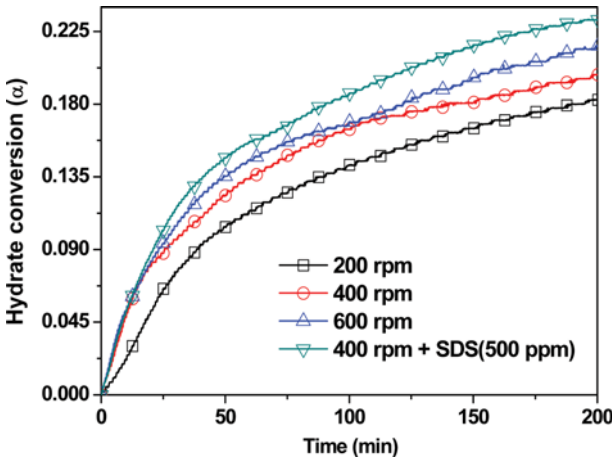

Fig. 7. Water to hydrate conversion during hydrate formation in stirred tank reactor at different stirring speeds (200, 400 and 600 rpm) and in presence of surfactant SDS at 400 rpm.

porous medium. The third growth stage is the slowest where crystallization process almost ceases due to extensive hydrate growth in the interspaces, thus limiting further contact of fresh water and gas phase. As seen in Fig. 6, the Avrami exponent n value of the system reduces to around 0.7 after first stage of growth and to 0.2 after second stage, which can be attributed to the slower conversion rates for hydrate formation in silica gel (100-200 mesh size) after certain hydrate conversion was achieved.

Hydrate formation in stirred tank reactor was performed for formation of CO_2 hydrates which form sI hydrate. Different stirring conditions (200-600 rpm) and promoters (SDS at 400 rpm) were taken to investigate their effect on Avrami parameters. The results obtained from the experiments are shown in Fig. 7. As seen there, the initial rate of CO_2 uptake (water to hydrate conversion, α) increases with increase in stirring, which clearly shows that with mass transfer the resistance decreases with stirring, thus reducing the film resistance. However, as discussed in literature, very high stirring speed may not necessarily reduce the film resistance as initial rate of hydrate formation is almost similar for a stirring speed of 400 rpm and 600 rpm. Addition of small amount of surfactant (500 ppm SDS concentration) reduces the surface tension and thus reduces the mass transfer limitation to certain extent. The results can be clearly seen on the hydrate formation kinetics, which shows better hydrate formation rate compared to the one obtained with no surfactants. Figs. 8 and 9 show the typical Avrami plot (Sharp Hancock plot) and correlation plot to measure the conversion ratio in stirred tank reactor. Table 1 summarizes the data calculated using the Avrami equation (n and k value). As seen in Fig. 8, it shows a perfect linear correlation with the experimental data in both the cases (with surfactant and without surfactant) with a correlation coefficient (R^2) of more than 0.99. As seen in Fig. 9, Avrami model fits the hydrate conversion ratio well during stage I of growth (refer Table 2 for MAPE). The calculated hydrate conversion using Avrami equation over-estimates the data after a certain hydrate conversion ratio (~0.15). Stage II of hydrate growth is limited by the diffusion through hydrate film. In a stirred tank reactor, hydrate formation gets enhanced due to vigorous stirring. As shown in Table 1, the

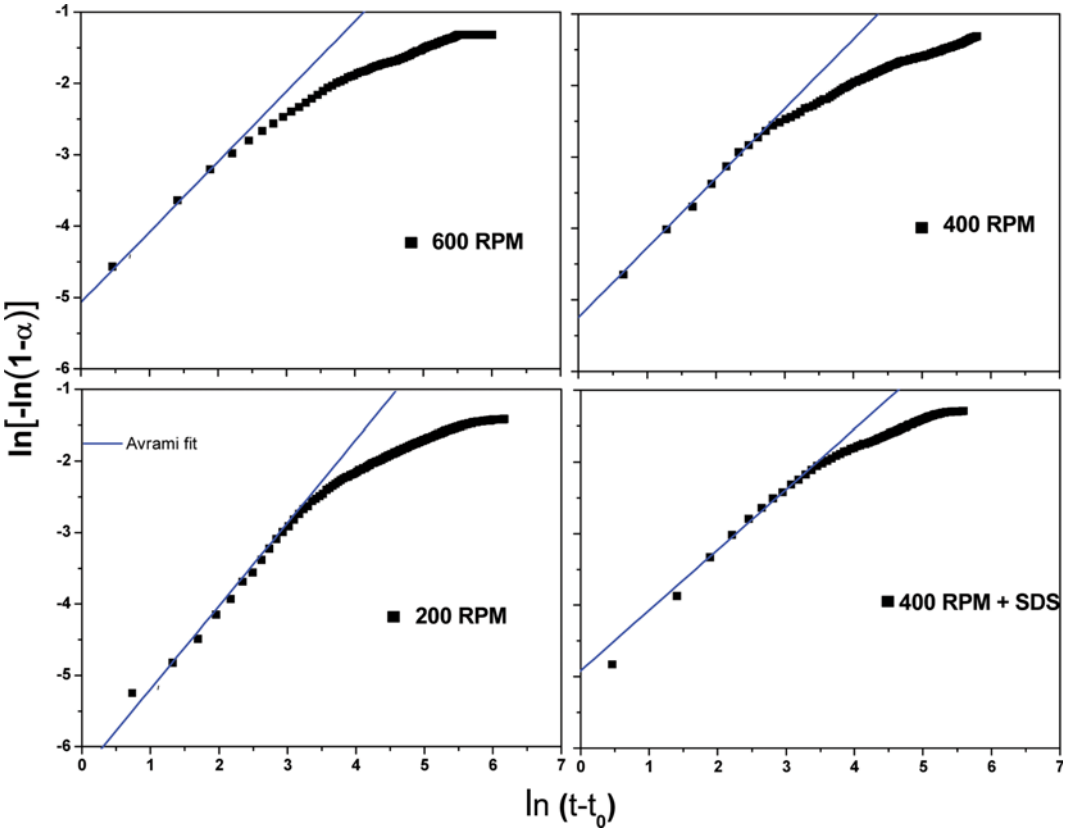

Fig. 8. Avrami plot for stirred tank reactor where three types of stirring speeds were used. Dotted line corresponds to the data calculated using Avrami equation and solid line corresponds to the linear fit. The regressed parameters (n and k) are given in Table 1.

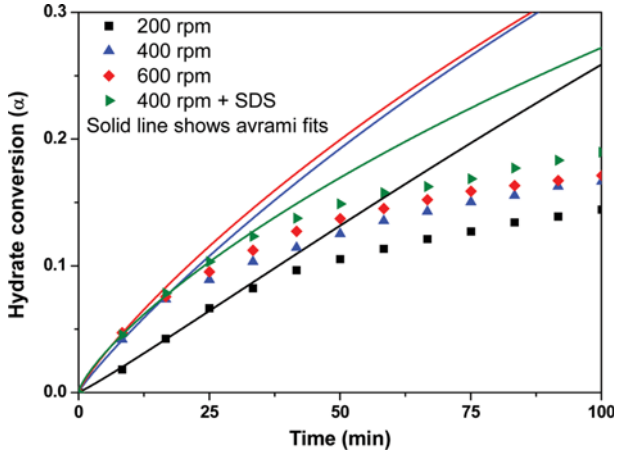

Fig. 9. Avrami plot for stirred tank reactor at different stirring rate, in which CO_2 hydrate was formed with and without surfactant; inset figure shows the water to hydrate conversion correlation with Avrami model for first 80 minutes.

value of n for CO_2 hydrate in a stirred tank reactor is closer to 1 (n=0.98 to 1.1), which suggests that almost no gas diffusion resistance exists for the first few minutes of hydrate formation in a stirred tank reactor, and hydrate formation is mostly one dimensional. This observation was also noted by Takeya et al. [44] and Uchida et al. [45] who reported that CO_2 hydrate crystal growth was initiated by hydrate formation at the interface between gas and water, and then hydrate crystals were observed to grow downward from the film in dendritic or needle-like shape.

Surprisingly, in presence of surfactant the Avrami exponent n value decreases to 0.84; similar results were also observed in a packed bed system. The expected n value was near to one because of increase in rate of hydrate formation on adding surfactant; however, this was not seen, which can be attributed to the high initial rate of hydrate formation which reduces the gas to water contact [46]. The regressed values of Avrami rate constant k are shown in Table 1. As expected from experimental results, the difference in rate constant k values for 400 rpm, 600 rpm and with surfactant experiments is not large. If we compare the rate in packed bed and stirred tank system (based on k value), these two systems are distinguishable as k value (initial rate) is higher in stirred tank system compared to packed bed system.

Fig. 10 represents the comparison of crystallization rate constant (k) data obtained from various systems such as stirred tank reactor (this work), fixed bed reactor (this work and Nambiar et al. [31]) and for ice powder (where hydrates were formed in ice using methane gas and tert-butyl methyl ether as sH hydrate former). When ice is exposed to methane gas, it forms sI hydrate; however, in the presence of large molecule guest substances (LMGS), it forms sH [30]. It is surprising that the crystallization rate in ice powder for sH is significantly high compared to sI (CH_4, CO_2, CO_2/H_2) and sII hydrates (CO_2/H_2/C_3H_8) in various media (silica sand,

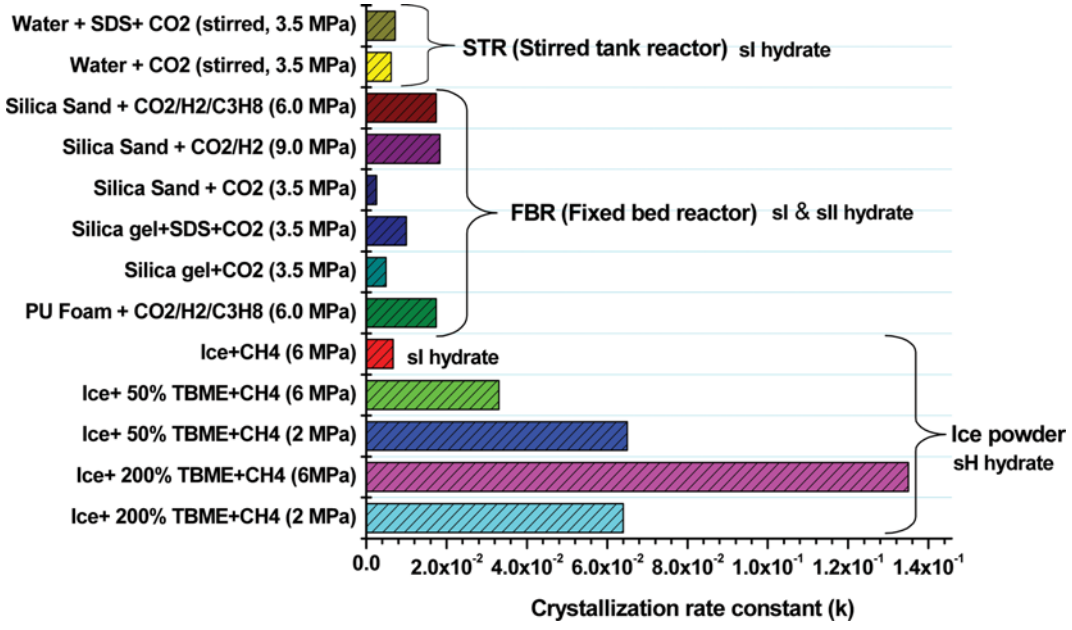

Fig. 10. Comparison of crystallization rate constant (k) data obtain from various systems such as stirred tank reactor (this work), fixed bed reactor (this work and Abhishek et al. [31]) and ice powder (hydrate formed in ice) Susilo et al. [30].

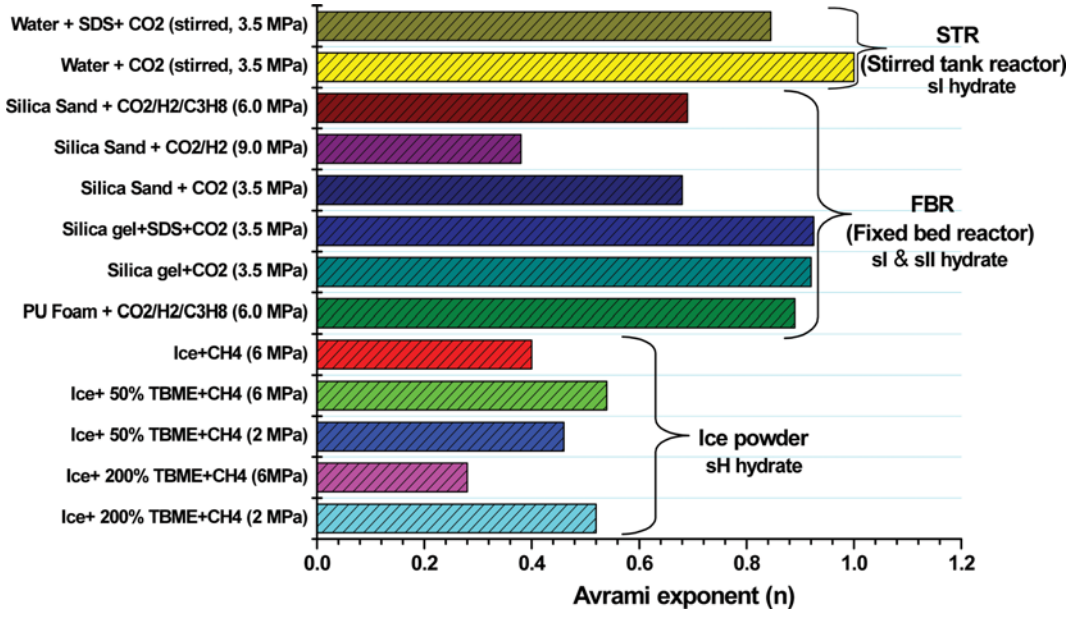

Fig. 11. Comparison of Avrami exponent (n) data obtain from various systems such as stirred tank reactor (this work), fixed bed reactor (this work and Abhishek et al. [31]) and ice powder (hydrate formed in ice) Susilo et al. [30].

silica gel, PU foam and ice powder) and STR. As can be seen in the figure, in the case of sH, when TBME concentration increases, there is a significant rise in rate at high pressure (6.0 MPa). This can only be explained on the basis of higher driving force available for hydrate formation in sH hydrate. Fig. 11 represents the comparison of Avrami exponent data obtained from various systems such as stirred tank reactor (this work), fixed bed reactor (this work and Nambiar et al. [31]) and for ice powder (when hydrates were formed in ice) [30]. As can be seen in the figure, the Avrami exponent shows different values for different systems. In ice powder, it is significantly less compared to STR and fixed bed systems. Additionally, when hydrates were formed from a ternary gas mixture ($CO_2/H_2/C_3H_8$) in fixed bed setup there was a significant difference in the slopes (n-value) for different gases. Avrami exponent was found to be 0.68 and 0.38 for sand/CO_2 (3.5 MPa pressure) and sand/CO_2/H_2 (9 MPa pressure) system, respectively, which reveals that Avrami exponent value depends on guest gas and experimental pressure.

CONCLUSION

The water to hydrate conversion rates in first stage of hydrate growth were well correlated by the Avrami equation. The Avrami exponent for fixed bed media and stirred tank was found to be ~0.9, which suggests linear hydrate growth in one dimension in rod- to disk-like crystal; this kind of crystal growth results from mass transfer limitation in highly confined pores of a fixed bed setup. For hydrate formation from ice, the Avrami exponent is even lower (~0.6); however, the rate of hydrate formation is quite fast compared to STR or fixed bed setup. This result points to the fact that conversion of ice to hydrate is a different mechanism and cannot be compared with classical nucleation and growth of crystal from a supersaturated system as in STR or fixed bed setup.

For gas hydrate system it is observed that:

a) Avrami plot fits quite well the initial rate of hydrate growth; however, with time due to more mass transfer resistance the Avrami equation fails to predict the growth rate. Higher mass transfer is seen in STR compared to a fixed bed setup.

b) In a fixed bed system Avrami type plots show a linear fit over all conversions but have non-integer values of slope. This is inconsistent with theory, which may be due to

1) Different nucleation mechanisms
2) Different kinds of spherulite (spherical semicrystalline regions)
3) Mass transfer effect
4) Rod to disk to spherulite conversion.

The Avrami exponent "n" may explain the hydrate nucleation and growth mechanism. This model is quite useful. As the morphology of hydrate growth in a packed bed medium cannot be observed visually, the parameter of the Avrami equation gives an idea of its growth. This kind of analysis will help to elucidate the growth kinetics of CO_2 hydrate during its sequestration in geological sites.

ACKNOWLEDGEMENTS

Authors gratefully acknowledge the financial support received from the Council of Scientific and Industrial Research (CSIR) & (Tap Coal: CSC 0102). A.K. acknowledges CSIR for providing a senior research fellowship (SRF).

REFERENCES

1. C. A. Koh, *Chem. Soc. Rev.*, **31**, 157 (2002).
2. E. D. Sloan and C. A. Koh, *Clathrate Hydrates of Natural Gases*, CRC Press, Boca Raton, Florida (2008).
3. P. Englezos, *Ind. Eng. Chem. Res.*, **32**, 1251 (1993).
4. G. Bhattacharjee, A. Kumar, T. Sakpal and R. Kumar, *ACS Sustainable Chem. Eng.*, **3**, 1205 (2015).
5. A. Kumar, T. Sakpal and R. Kumar, *Chem. Eng. Sci.*, **122**, 78 (2015).
6. D. Aaron and C. Tsouris, *Sep. Sci. Technol.*, **40**, 321 (2005).
7. P. Babu, P. Linga, R. Kumar and P. Englezos, *Energy*, **85**, 261 (2015).
8. S. P. Kang and H. Lee, *Environ. Sci. Technol.*, **34**, 4397 (2000).
9. S. D. Kenarsari, D. Yang, G. Jiang, S. Zhang, J. Wang, A. G. Russell, Q. Wei and M. Fan, *RSC Adv.*, **3**, 22739 (2013).
10. P. Linga, R. Kumar and P. Englezos, *Chem. Eng. Sci.*, **62**, 4268 (2007).
11. A. Kumar and R. Kumar, *Energy Fuels*, **29**, 4463 (2015).
12. P. Babu, R. Kumar and P. Linga, *Environ. Sci. Technol.*, **47**, 13191 (2013).
13. S. M. Kim, J. D. Lee, H. J. Lee, E. K. Lee and Y. Kim, *Int. J. Hydrogen Energy*, **36**, 1115 (2011).
14. X. S. Li, C. G. Xu, Z. Y. Chen and H. J. Wu, *Energy*, **36**, 1394 (2011).
15. P. Linga, R. Kumar and P. Englezos, *J. Hazard. Mater.*, **149**, 625 (2007).
16. A. Adeyemo, R. Kumar, P. Linga, J. Ripmeester and P. Englezos, *Int. J. Greenh. Gas Control*, **4**, 478 (2010).
17. P. Babu, R. Kumar and P. Linga, *Energy*, **50**, 364 (2013).
18. Y. Seo and S. P. Kang, *Chem. Eng. J.*, **161**, 308 (2010).
19. Y. T. Seo, I. L. Moudrakovski, J. Ripmeester, J. W. Lee and H. Lee, *Environ. Sci. Technol.*, **39**, 2315 (2005).
20. D. Kashchiev and A. Firoozabadi, *J. Cryst. Growth*, **250**, 499 (2003).
21. P. R. Bishnoi and V. Natarajan, *Fluid Phase Equilib.*, **117**, 168 (1996).
22. P. Skovborg and P. Rasmussen, *Chem. Eng. Sci.*, **49**, 1131 (1994).
23. D. Sun and P. Englezos, *Int. J. Green. Gas Control*, **25**, 1 (2014).
24. M. Avrami, *J. Chem. Phys.*, **7**, 1103 (1939).
25. M. Avrami, *J. Chem. Phys.*, **8**, 212 (1940).
26. M. Avrami, *J. Chem. Phys.*, **9**, 177 (1941).
27. D. Kashchiev and A. Firoozabadi, *J. Cryst. Growth*, **243**, 476 (2002).
28. I. L. Moudrakovski, A. A. Sanchez, C. I. Ratcliffe and J. Ripmeester, *Phys. Chem. B.*, **105**, 12338 (2001).
29. A. Falenty and W. F. Kuhs, *J. Phys. Chem. B.*, **113**, 15975 (2009).
30. R. Susilo, J. Ripmeester and P. Englezos, *AIChE J.*, **53**, 2451 (2007).
31. A. Nambiar, P. Babu and P. Linga, *Canad. J. Chem.*, **93**, 808 (2015).
32. U. W. Gedde, *Polymer Physics: Crystallization Kinetics*, Chapman and Hall, London (1995).
33. A. G. Marangoni, *Fat Crystals Network: Crystallization Kinetics*, Marcel Dekker, New York (2005).
34. A. Shaples, *Introduction to Polymer Crystallization,* Edward Arnold, London (1966).
35. A. Kumar, T. Sakpal, P. Linga and R. Kumar, *Fuel*, **105**, 664 (2013).
36. A. Kumar, T. Sakpal and R. Kumar, *Energy Technol.*, **3**, 717 (2015).
37. R. Serna-Guerrero and A. Sayari, *Chem. Eng. J.*, **161**, 182 (2010).
38. J. Wang, L. A. Stevens, T. C. Drage and J. Wooda, *Chem. Eng. Sci.*, **68**, 424 (2012).
39. A. T. Lorenzo, M. L. Arnal, J. Albuerne and A. J. Müller, *Polym. Test.*, **26**, 222 (2007).
40. E. Piorkowska, A. Galeski and J. M. Haudin, *Prog. Polym. Sci.*, **31**, 549 (2006).
41. J. Mark, K. Ngai, W. Graessley, L. Mandelkern, E. Samulski, J. Koenig and G. Wignall, Physical Properties of Polymers, 3rd, Cambridge University Press, Cambridge (2004).
42. J. M. Shultz, Polymer Crystallization, Oxford U. P., Oxford (2001).
43. P. Babu, D. Yee, P. Linga, A. Palmer, B. C. Khoo, T. S. Tan and P. Rangsunvigit, *Energy Fuels*, **27**, 3364 (2013).
44. S. Takeya, A. Hori, T. Hondoh and T. Uchida, *J. Phys. Chem. B.*, **104**, 4164 (2000).
45. T. Uchida, T. Ebinuma, J. Kawabata and H. Narita, *J. Cryst. Growth*, **204**, 348 (1999).
46. A. Kumar, G. Bhattacharjee, B. D. Kulkarni and R. Kumar, *Ind. Eng. Chem. Res.*, **54**, 12217 (2015).